Journal of Al Azhar University-Gaza (Natural Sciences), 2012, 14: 111-138

Geochemistry and petrogenesis of El-Fringa metagabbro-diorite rocks, Wadi Sa'al area, south Sinai, Egypt

Nedal Qaoud[1], Amr Abdelnasser[2]

1 Department of Geology, Al Azhar University-Gaza,Palestine
2 Department of Geology, Faculty of Science, Benha University, 13518, Egypt

Received 10/7/2012 Accepted 24/10/2012

Abstract:
Neoproterozoic metagabbro-diorite-tonalite intrusive complexes (~881±58 Ma) of the basement complex of the Egyptian Eastern Desert and Sinai represent subduction-related magmatic edifice in the early stages of the Pan-African orogeny. These rocks exhibit petrological and geochemical characteristics of island arc-related magmas derived possibly from partial melting of a mantle wedge above a subduction zone or originated from partial melting of an amphibolitic lower crust by anatexis process at a volcanic arc regime. The El-Fringa metagabbro-diorite complex crops out at the northwest district of Wadi Sa'al and cuts the structural grain of the Sa'al metavolcanic group. It is composed of heterogeneous mafic and intermediate rock varieties, namely: hornblende metagabbro diorite to and quartz-diorite. Geochemically, this complex has transitional tholeiitic- and calc-alkaline magma. It is suggested that this complex was probably formed by fractional crystallization of a basaltic magma derived by partial melting of a metasomatised upper mantle in an island-arc setting.

The REE patterns of the studied rocks are more or less identical, i.e., generally enriched light REE with variably distinct positive Eu anomalies, and depleted heavy REE. The systematic increase in total REE abundances from least to most evolved gabbro and diorite varieties, which can be explained in terms of fractional crystallization. Field relationships, tectonic setting, mineralogical and geochemical characteristics of the El-Fringa complex are comparable with similar suits in the Eastern Desert and may represent a concomitant island arc magmatic increment.

Keyword: *Metagabbro-diorite complex, Geochemistry, Island arc rocks, El-Fringa, Sinai, Egypt.*

Introduction:

The Arabian-Nubian Shield is characterized by the abundance of volcanosedimentary successions of greenschist facies metamorphism, dismembered ophiolitic complexes, gabbro-diorite-tonalite complexes and unmetamorphosed volcanic and pyroclastic sequences that are extensively intruded, particularly in the northern Eastern Desert of Egypt, by batholithic granodiorite-granite complexes (El Ramly, 1972; Vail, 1985).

The mafic plutonic rocks of the Egyptian shield (mostly of gabbroic composition) were earlier classified by Akaad and El Ramly (1960) into two major groups: older gabbros and post-orogenic younger gabbros. They also recently subdivided into three distinct groups (e.g. Hassan and Hashad, 1990); (1) ophiolitic gabbro association which is considered to be a syn-orogenic suite; (2) metagabbro-diorite which form an integral part of the ophiolitic sequences in the Nubian Shield; and (3) unmetamorphosed post-orogenic younger gabbros. The metagabbro-diorite complex is of wider distribution and form relatively large outcrops in the Eastern Desert and Sinai compared with the younger gabbros. Their emplacement occurred at around 987-830 Ma (Hashad, 1980; Abdel Rahman and Doig, 1987). Thus, they represent the earliest phase of crustal growth in the Nubian Shield of Egypt (Abdel Rahman, 1990). K-Ar age dating of the hornblendes and biotites separated from the metagabbro-diorite complex of Wadi Baba, South-west Sinai gave 794+30 - 667+25 Ma age which corresponds to the late Precambrian arc magmatism in the Arabian-Nubian shield (Abdel-Karim, 1995).

In Sinai Peninsula, the mafic-ultramafic intrusions crop out as numerous small masses and occur in several areas such as Wadi Melhega, Wadi El Bida, Wadi Nesryin, Wadi Feiran, Wadi El Akhdar, Wadi Sa'al and Wadi El Mahash (Fig. 1). They were metamorphosed into the green-schist facies, and locally in the lower amphibolites. These intrusions intruded in an active continental margin above subduction zone (El Metwally, 1997), thus their emplacement occurred during the late- to post-orogenic stage of the Pan-African orogeny (El Metwally, 1993; Essawy et al. 1997) during the late Cordilleran stage (655–570 Ma, El Gaby et al. 1988) and coeval with the syn- to late orogenic calc-alkaline (G_1-G_2) granites. The Melhega

metagabbro-diorite complex in southeastern Sinai originated from magmas related to a subduction zone in a transitional ocean floor to arc environment (Hassanen, 1989). As well as, the gabbroic rocks of El Mahash, El Bida, Feiran, Sa'al and Melhega at southern Sinai composed mainly of oxyhornblende gabbro, olivine gabbro, pyroxene hornblende gabbro, leucogabbro and gabbro-norite and exhibit chilled margins at their contact with the country rocks that are represented by fine-grained fresh gabbro-norite and oxyhornblende gabbro (Madbouli, 1991). According to Basta (1998), the gabbroic intrusions of Melhega, Sa'al and Watier areas were formed from a calc-alkaline magma in an active continental margin setting. Takla et al. (2001) considered the most mafic-ultramafics of south Sinai as non-ophiolitic assemblage belonging to the Egyptian Younger Gabbros.

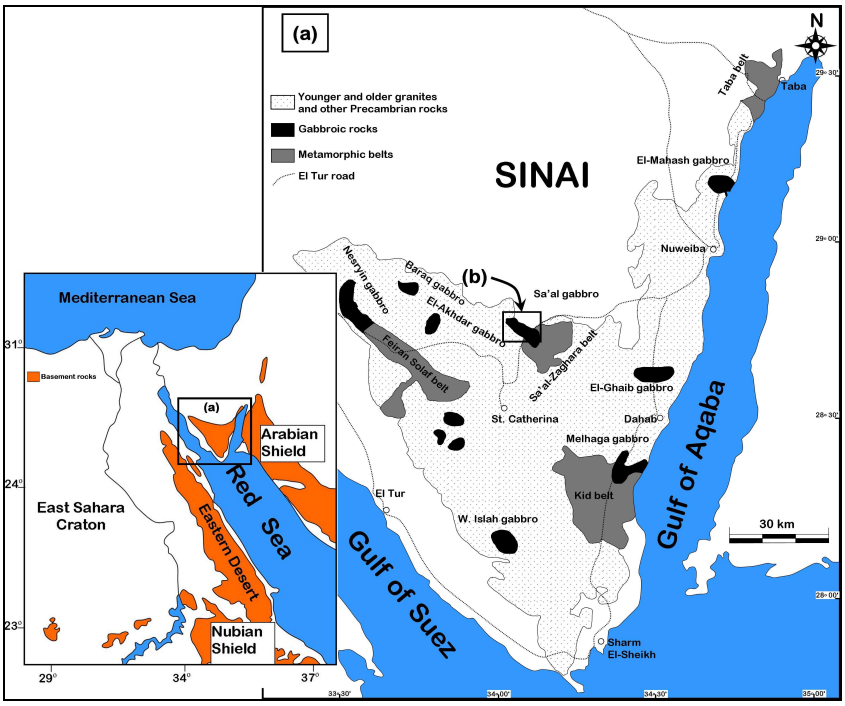

Fig. (1): Distribution of Precambrian basement exposures on both sides of the Red Sea. (a) Sketch map showing the location of gabbroic rocks and other main Precambrian rock units in southern Sinai.

The area under investigation is a part of the Pan-African basement rocks in South Sinai of Egypt (Fig. 2) that located at the northwest

district of Wadi Sa'al and forms moderately and rugged outcrops of new Proterozoic igneous and metamorphic rocks. The mapped area is delineated between lat. 28º 42' 00" and 28º 46' 00" N and long. 34º 02' 00" and 34º 10' 00" E, and covers approximately 110 km^2 (Fig. 2).

This work introduces geologic setting combined with the petrographical and geochemical investigations for El-Fringa metagabbro-diorite complex at the study area. The main aim is to better understand plausible petrogenesis and tectonic setting of these rock types.

Geologic setting, field relationships and petrography

The study area is underlain mainly by metagabbro-diorite intrusive complex intruded in Sa'al metavolcanics and metasediments and latter intruded by late- to post-tectonic granitoid rocks (Fig. 2). The Sa'al metavolcanics range in composition from mafic (basalt) to felsic (rhyolite) and which comprise a wide variety of rock types such as andesite, dacite, and rhyolite with minor basalt bodies. Bielski (1982) gave Rb-Sr whole rock ages of 734±17 Ma for these metavolcanic rocks. At Wadi El-Raiyan, these metavolcanics are mostly acidic in composition with subordinate amount of intermediate and basic metavolcanic rocks. The acidic metavolcanic rocks are characterized by calc-alkaline to sub-alkaline in nature and regionally metamorphosed up to the greenschist facies. They are related to the calc-alkaline island arc metavolcanics of the central Eastern Desert of Egypt (Bentor, 1985).

Tuffaceous metavolcanic rocks which are mostly metarhyolitic rocks are concentrated in the southeastern part of the study area (Fig. 2). They are tectonically bounded by other metavolcanic bodies with well-foliated features.

The metavolcanics are interbedded with volcanogenic metasediments which mainly occur in the northern part of Wadi Sa'al area (Fig. 2).

The clastic metasediments are represented by Zaghra conglomerate occurring as small area at Wadi El-Raiyan (Fig. 2) and were originally sediments deposited under subaqueous conditions in fluvial environment (Hassen et al. 2004). They are highly deformed and metamorphosed to greenschist facies of a low-grade metamorphism.

The main types of this Zaghra conglomerate are differentiated into volcanic pebbles (mainly andesite, rhyolite and tuffs) and granitic pebbles (mainly granodiorite).

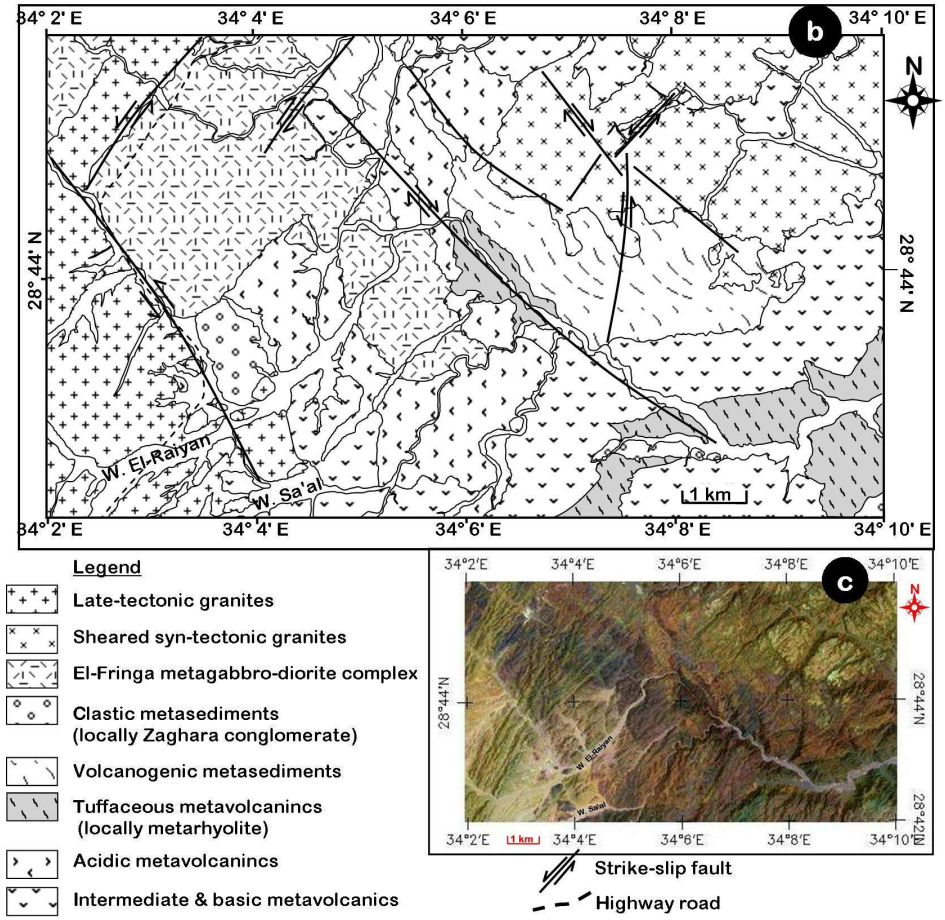

Fig. 2: b) Geological map of the basement complex of Wadi El-Raiyan area, South Sinai, Egypt. (Modified after Hassen et al. 2004). c) Landsat ETM+ ratio image with 7, 4, 1 for Red-Green-Blue of the study area.

The investigated metagabbro-diorite complex forms an elongate isolated exposure of moderate to high relief, trending NW-SE, occupying about 20 Km^2. At the start and north of Wadi El-Raiyan, this complex occurs as a small stock and intrudes Sa'al metavolcanics. It surrounds the voluminous granite of Wadi Saal forming a nearly circular stock-like intrusion (Fig. 2). It has irregular and sharp intrusive contacts with its country rocks and cut by numerous quartz

and veins and aplite dikes and pegmatites. Based on the color index, textures and mineral proportions, this complex is represented by heterogeneous mafic and intermediate rock varieties comprising hornblende metagabbro and diorite to quartz-diorite rocks.

The hornblende metagabbros are coarse-grained holocrystalline rocks and exhibit hypidiomorphic granular texture. They consist mainly of calcic plagioclase, hornblende, pyroxene with subordinate amount of biotite and quartz. Ilmenite, magnetite, apatite and pyrite are accessories. These rocks were subjected to regional metamorphism within greenschist facies conditions, where calcic plagioclase are commonly replaced by saussurite albite and ferromagnesian minerals partially replaced by actinolite as well as chlorite associated with opaque minerals and titanite (Fig 3a). The coexisting mineral assemblage actinolite, epidote, chlorite and opaques usually represent low pressure metamorphism (Miyashiro 1974).

Plagioclase ($An_{62–71}$) forms subidiomorphic to xenomorphic crystal, locally laths and partly saussuritized. Its alteration is either in the crystal core or on the peripheries causing masking for lamellar twinning (Fig. 3b). Cracking and bending of twin lamellae are occasionally recorded as signs of deformation. Plagioclase zoning is sometimes observed (Fig. 3c).

Clinopyroxene (28% vol. %) partially altered to actinolite and tremolite with subordinate chlorite and uralite, and forming ophitic and subophitic textures with plagioclase (Fig. 3a and d). The opaque minerals may be either exsolved iron oxide, or a late magmatic reaction product associated with clinopyroxene (Fig. 3a). Uralitic amphibole is generally fibrous; (Fig. 3e) displays more gradational contacts with clinopyroxene, and probably originates from deuteric volatiles or fluids permeating the completely crystallized rock.

The amphiboles are represented by hornblende and actinolite with subordinate uralite. Hornblende forms prisms, plates and irregular aggregates and shows yellow, yellowish brown to deep brown in color and strongly pleochroic. It is poikilitically enclosed laths of plagioclase as well as iron oxides and altered to actinolite, chlorite and sometimes epidote. Actinolite is the main secondary amphibole minerals, pale green to slightly colorless and occurs as shreds, fibrous

and rim surrounded the clinopyroxene cores with rare amount of tremolite. In some thin section, the intense alteration of clinopyroxene of the studied metagabbros resulted in the formation of rocks-rich in actinolite with subordinate uralite and zoisite beside saussuritized plagioclase (Fig. 3f).

The diorite occurs as a medium- to fine-grained (0.7 to 0.1 mm) rock consisting essentially of plagioclase (andesine to oligoclase in composition) and green hornblende with subordinate actinolite and minor biotite, iron-titanium oxides, titanite and epidote. Quartz is subordinate, and rare relict cores of clinopyroxene in large hornblende crystals have been observed in some samples. Plagioclase forms euhedral and subhedral lath-like crystals containing inclusions of epidote and sometimes zoned. It also occurs as inclusions observed in biotite flakes. Plagioclase and epidote form clusters surrounding the former minerals.

The hornblende is strongly pleochroic from light bluish green to pale green and partially altered to chlorite. Most of the magnetite and titanite are partially altered to hematite and leucoxene respectively.

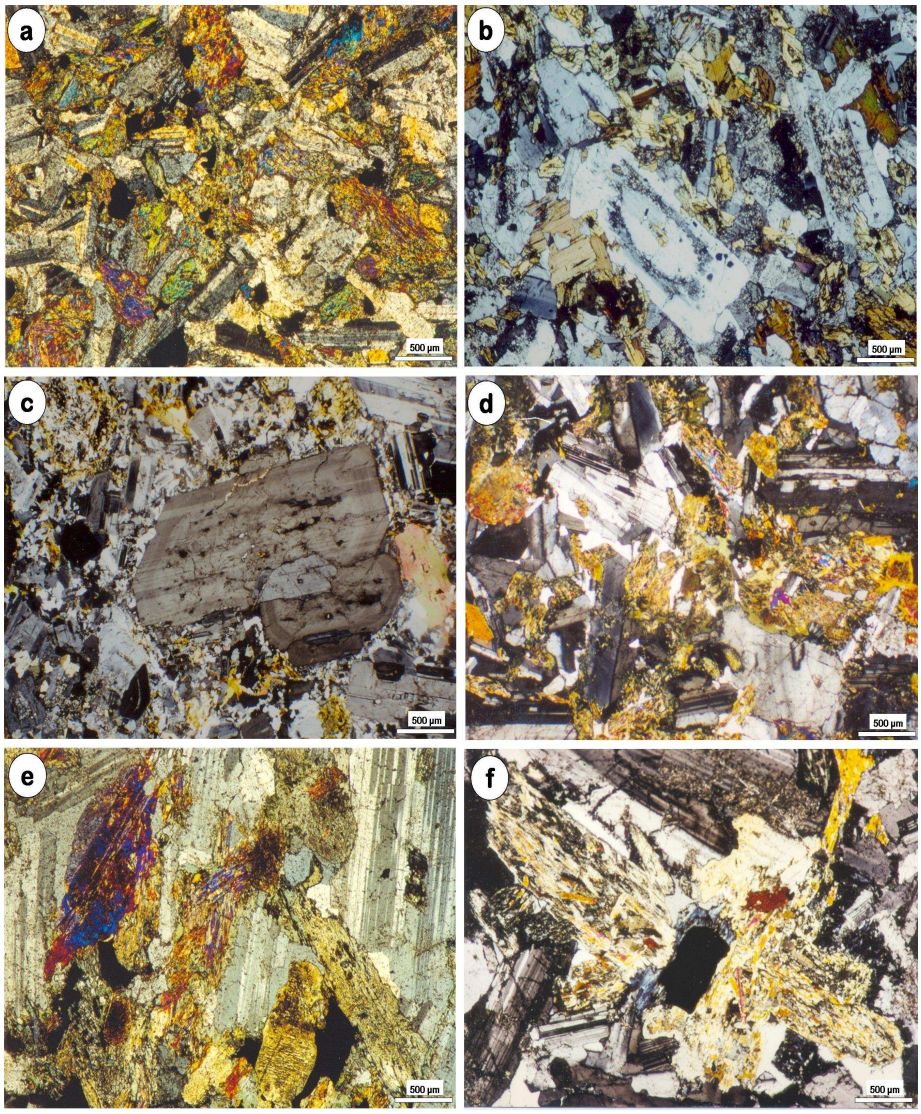

Fig. (2): Photomicrograph of hornblende metagabbros showing; a) Saussuritized plagioclase associated with Altered pyroxene, actinolite and exsolved Fe-oxide. b) Saussuritization alteration in plagioclase. c) Large crystal of zoned plagioclase. d) Pseudo ophitic and subophitic textures of plagioclase, tremolite-actinolite and subordinate uralite and pyroxene relics. e) Uralitic amphibole after clinopyroxene. f) Tremolite-actinolite with subordinate zoisite and opaque minerals.

Geochemistry

Twenty-two rock samples of the metagabbro-diorite complex were analyzed for the major oxides and some trace and rare earth elements (REE) by using ICP-MS at the Technical University of Budapest, Hungary. The analytical error for the major elements is 2% and for trace elements is mostly less than 10%. Rare earth elements concentrations have been normalized to chondrite after Nakamura (1974). The major, trace and rare earth elements and CIPW norm are listed in Tables 1 & 2.

Based on the field evidence, petrographic studies and geochemical data of the studied El-Fringa metagabbro-diorite complex, these rocks may be divided according to their specific features into two groups; metagabbro and diorite. Geochemically, the studied metagabbros have markedly enrichment in TiO_2, Fe_2O_3, MgO and CaO contents relative to those of diorite, whereas it has low contents of Al_2O_3, SiO_2 and K_2O than diorite. On the other hand, the metagabbros show depletion in Ti/Cr ratio than those of diorite, the rocks are characterized by high Mg# of 0.71 for metagabbro and 0.67 for the diorite.

El-Fringa metagabbro diorite complex has geochemical characteristics of medium-to high-K calc-alkaline arc series as defined by Gill (1981), De La Roche et al. (1980) and Peccerillo and Taylor (1976) (Fig. 4a), typical for arcs swinging between primitive island arc tholeiites to calc-alkaline volcanics during arc polarity reversal (Pindell and Kennan, 2001).

The alkali versus SiO_2 diagram (Cox et al., 1979) confirmed that the metagabbros classified as subalkalic gabbro with only two samples having an elevated total alkalies value falls in the alkali-gabbro region. While, the diorite rocks are subdivided as subalkalic diorite and quartz diorite with alkali syeno-diorite (Fig. 4b).

Table (1): Major and trace elements and CIPW norm of metagabbros of the study area

	14-G	15-G	16-G	17-G	18-G	19-G	20-G	21-G	22-G
SiO_2	51.38	49.7	47.96	47.96	47.42	46.94	45.98	45.26	44.48
TiO_2	1.09	0.47	0.52	1.25	0.99	1.16	0.35	1.38	2.11
Al_2O_3	18.56	19.68	17.76	17.78	20.12	17.7	24.86	22.14	18.47
Fe_2O_3	7.98	6.42	9.29	11.98	10.71	10.59	6.42	11.95	11.94
MnO	0.14	0.12	0.16	0.13	0.15	0.13	0.09	0.12	0.16
MgO	4.93	7.18	8.62	5.79	6.58	6.54	5.49	4.34	5.21
CaO	9.68	12.95	11.15	10.59	10.32	12.18	13.64	10.18	11.35
Na_2O	3.58	1.85	2.07	2.39	2.41	2.69	1.82	2.55	3.06
K_2O	0.84	0.27	0.5	0.87	0.24	0.18	0.21	0.72	0.61
P_2O_5	0.28	0.09	0.28	0.11	0.02	0.15	0.05	0.06	0.22
Na_2O+K_2O	4.42	2.12	2.57	3.26	2.65	2.87	2.03	3.27	3.67
$FeO^{\{t\}}$	7.35	5.89	8.58	11.04	9.84	9.80	5.88	11.03	11.03
$FeO^{\{t\}}$/Mgo	1.49	0.82	1.00	1.91	1.50	1.50	1.07	2.54	2.12
Trace elements (ppm)									
Ba	240	210	208	152	228	301	393	116	149
Rb	23	6	14	19.6	5	24	6	24	12
Sr	886	719	681	671	860	611	1000	912	943
Y	17	9	11	13	11	19	3	14	16
Zr	94	41	33	65	34	80	25	70	66
Cr	111	192	200	97	130	86	107	199	45
Ni	23	69	75	38	51	40	26	51	10
Co	26	36.7	47	56	43	35	31.5	49	31
Sc		32	40	31	30	87	21		38
V	118	130	200	205	320	200	120	206	296
Cu	11	60	116	70	15	17	87	49	19
Pb	14	20	21	14	20	11	20	14	11
Zn	92	52	100	55	108	73	55	119	112
Cs	-	1.22	1.5	1.59	0.84	0.29	1	-	0.91
Th	-	0.8	-	3.18	0.9	1.58	1	-	0.61

U	-	-	-	**1.33**	-	**1.11**	-	-	**0.7**
La	**10.29**	**5.52**	**4.9**	**8.91**	**7.67**	**8.83**	**8.19**	**10.11**	**16.19**
Ce	**25.43**	**9**	**10.1**	**20.59**	**9.6**	**21.01**	**11**	**24.14**	**39.02**
Nd	**16.5**	**8**	**8**	**13.04**	**8**	**11.55**	**7**	**16.77**	**25.53**
Sm	**2.91**	**1.86**	**1.88**	**3.27**	**2.16**	**2.9**	**0.85**	**3.72**	**7.26**
Eu	**1.16**	**0.72**	**0.8**	**1.09**	**0.74**	**0.92**	**0.51**	**0.6**	**1.51**
Gd	**7.22**	**3.2**	**2.5**	**2.44**	**2.2**	**2.52**	**2.1**	**2.12**	**6.36**
Tb	**0.51**	**0.29**	**0.66**	**0.42**	**0.51**	**0.32**	**0.31**	**0.39**	**1.08**
Tm	**0.51**	**1.38**	**0.47**	**0.44**	**1.39**	**0.45**	**1.35**	**0.41**	**1.08**
Yb	**1.26**	**0.83**	**1.05**	**1.39**	**0.79**	**1.11**	**0.32**	**1.21**	**2.24**
Lu	**0.24**	**0.23**	**0.27**	**0.22**	**0.24**	**0.18**	**0.21**	**0.2**	**0.36**
Σ REE	**66.03**	**31.03**	**30.63**	**51.81**	**33.30**	**49.79**	**31.84**	**59.67**	**100.63**
Σ LREE	**52.22**	**22.52**	**23.00**	**42.54**	**25.27**	**41.39**	**26.19**	**51.02**	**80.74**
Σ MREE	**11.80**	**6.07**	**5.84**	**7.22**	**5.61**	**6.66**	**3.77**	**6.83**	**16.21**
Σ HREE	**2.01**	**2.44**	**1.79**	**2.05**	**2.42**	**1.74**	**1.88**	**1.82**	**3.68**
Eu/Eu*	**0.78**	**0.91**	**1.13**	**1.19**	**1.04**	**1.05**	**1.17**	**0.66**	**0.68**
Sr/Sr*	**0.35**	**0.70**	**0.62**	**0.34**	**0.80**	**0.32**	**0.93**	**0.37**	**0.25**
Zr/Zr*	**0.07**	**0.05**	**0.04**	**0.05**	**0.04**	**0.07**	**0.05**	**0.04**	**0.02**
(La/Lu)n	**4.42**	**2.47**	**1.87**	**4.17**	**3.29**	**5.05**	**4.02**	**5.21**	**4.63**
(La/Yb)n	**5.44**	**4.43**	**3.11**	**4.27**	**6.47**	**5.30**	**17.06**	**5.57**	**4.82**
(La/Sm)n	**2.18**	**1.83**	**1.60**	**1.68**	**2.18**	**1.87**	**5.93**	**1.67**	**1.37**
(Gd/Yb)n	**4.57**	**3.07**	**1.90**	**1.40**	**2.22**	**1.81**	**5.23**	**1.40**	**2.26**
(Tb/Yb)n	**1.89**	**1.64**	**2.94**	**1.41**	**3.02**	**1.35**	**4.53**	**1.51**	**2.26**
(Ce/Yb)n	**5.13**	**2.76**	**2.45**	**3.77**	**3.09**	**4.81**	**8.74**	**5.07**	**4.43**
"r"	**25.98**	**9.23**	**12.85**	**20.75**	**10.44**	**23.79**	**13.93**	**28.03**	**21.94**
Ti	**6449.70**	**2781.07**	**3076.92**	**7396.45**	**5857.99**	**6863.91**	**2071.01**	**8165.68**	**12485.21**
Ti/Cr	**58.11**	**14.48**	**15.38**	**76.25**	**45.06**	**79.81**	**19.36**	**41.03**	**277.45**
Mg# (mole %)	**0.71**	**0.82**	**0.79**	**0.66**	**0.71**	**0.71**	**0.77**	**0.59**	**0.63**
CIPW norm (wt %)									
Quartz	**0.72**	**1.49**	**0.00**	**0.00**	**0.00**	**0.00**	**0.00**	**0.00**	**0.00**
Orthoclase	**5.07**	**1.62**	**3.03**	**5.25**	**1.45**	**1.09**	**1.26**	**4.35**	**3.69**
Albite	**30.94**	**15.93**	**17.95**	**20.65**	**20.78**	**23.36**	**15.64**	**22.07**	**24.95**
Anorthite	**32.78**	**45.38**	**38.63**	**35.96**	**44.20**	**36.62**	**59.97**	**47.90**	**35.65**
Plagioclase	**63.71**	**61.31**	**56.58**	**56.62**	**64.98**	**59.97**	**75.62**	**69.96**	**60.60**

Nephline	**0.00**	**0.00**	**0.00**	**0.00**	**0.00**	**0.00**	**0.00**	**0.00**	**0.83**
Corundum	**0.00**	**0.00**	**0.00**	**0.00**	**0.00**	**0.00**	**0.00**	**0.00**	**0.00**
Diopside	**11.61**	**15.49**	**13.07**	**13.91**	**6.39**	**19.81**	**6.79**	**2.77**	**11.21**
Hypersthene	**12.28**	**16.06**	**14.65**	**12.51**	**15.13**	**1.94**	**3.76**	**2.88**	**0.00**
Pyroxene	**23.89**	**31.56**	**27.72**	**26.42**	**21.52**	**21.75**	**10.54**	**5.65**	**11.21**
Olivine	**0.00**	**0.00**	**8.00**	**4.96**	**6.42**	**10.62**	**9.07**	**12.95**	**11.33**
Magnetite	**3.84**	**2.91**	**3.00**	**4.07**	**3.68**	**3.96**	**2.72**	**4.27**	**5.35**
Ilmenite	**2.11**	**0.91**	**1.01**	**2.42**	**1.92**	**2.26**	**0.68**	**2.68**	**4.10**
Apatite	**0.66**	**0.21**	**0.66**	**0.26**	**0.05**	**0.36**	**0.12**	**0.14**	**2.89**

Table (2): Major and trace elements and CIPW norm of diorite rocks of the study area.

	1-D	**2-D**	**3-D**	**4-D**	**5-D**	**6-D**	**7-D**	**8-D**	**9-D**	**10-D**	**11-D**	**12-D**	**13-D**
SiO2	65.37	64.1	61.7	59.54	58.24	58.14	57.33	57	55.92	54.96	53.75	53.18	51.98
TiO2	0.48	0.84	0.96	1.02	0.93	1.03	1.02	0.87	0.73	0.99	1.88	1.15	0.86
Al2O3	16.6	15.75	15.8	16.5	17.96	16.93	17.64	16.94	17.28	17.29	18.29	19.54	17.56
Fe2O3	3.59	4.54	6.31	6.44	6.08	7.39	7.31	7.65	6.38	8.18	10.06	8.52	8.28
MnO	0.03	0.02	0.1	0.11	0.12	0.13	0.12	0.12	0.13	0.13	0.5	0.12	0.08
MgO	1.91	1.71	3.29	2.64	3.17	3.78	3.46	5.05	4.28	5.12	2.96	3.94	6.16
CaO	2.69	4.75	5.26	4.34	6.27	6.68	6.43	5.38	8.48	7.54	6.5	7.55	4.71
Na2O	4.56	5.13	3.88	4.22	4.64	3.49	3.77	3.24	4.06	3.85	4.43	4.14	4.68
K2O	3.34	1.19	1.71	2.51	1.49	1.55	1.67	2.57	0.79	0.76	1.59	0.97	3.26
P2O5	0.13	0.31	0.27	0.34	0.32	0.33	0.28	0.26	0.03	0.22	0.45	0.27	0.19
Na2O+K2O	7.90	6.32	5.59	6.73	6.13	5.04	5.44	5.81	4.85	4.61	6.02	5.11	7.94
FeO{t}	3.28	4.17	5.76	5.97	5.55	6.74	6.69	7.00	5.89	7.49	9.11	7.78	7.69
FeO{t}/Mgo	1.72	2.44	1.75	2.26	1.75	1.78	1.93	1.39	1.38	1.46	3.08	1.97	1.25
Trace elements (ppm)													
Ba	1076	515	549	377	340	436	540	854	600	370	713	380	908
Rb	61	28	46	36	29	46	47	75	46	18	32	21	50
Sr	786	704	614	514	1011	688	600	714	541	665	680	798	541

Y	23	17	18	26	21	25		37	23	15	22	12	23
Zr	211	100	224	149	120	155	176	180	226	129	97	64	225
Cr	40	40	115	67	56	147	37	251	66	143	22	43	120
Ni	45	34	44	39	31	48	24	79	40	67	29	24	21
Co	21	19	24	26	18	33	29.1	33	21	29.1	23	24.7	25
Sc	3.18	3.21	20	2		19	20	12.6	24	30	6.4	18.3	10
V	62.22	57	160	99	170	104	190	140	280	200	51	290	60
Cu	28	34	27	38	18	23	38	32	15	35	35	40	12
Pb	27	16	20	25	20	17	20	16	21	21	8	21	3
Zn	55	93	85	88	280	88	91	81	89	93	155	69	60
Cs	3.93	1.11	3	1.1	-	1.44	3.3	7	2.1	1.6	2	1.32	1.2
Th	8.68	1.31	6	5.2	4.7	6.3	3.7	3.8	-	2.6	1.16	4	4
U	2.06	1.81	1.1	1.7	1.3	1.61	-	1.12	-	-	0.09	-	1
La	34.12	12.93	19.75	26.31	20.8	25.33	18.9	19.76	30	16.3	20.31	9.5	17.9
Ce	63.4	29.74	31	46.4	45.88	58.6	33	43.24	20	26	47.31	9	21
Nd	21.94	8.74	17	22.1	24.96	35.47	16	33.09	6	26	29.41	9	15
Sm	33.5	3.42	3.88	4.11	5.62	4.94	4.42	5.57	2.44	3.48	7.66	2.68	4.78
Eu	0.08	1.09	1.2	0.88	1.73	1.3	1.36	1.43	1.03	1.25	1.97	1.11	1.21
Gd	1.24	1.25	2.6	2.5	5.08	3.74	21	8.41	23	8.5	8.51	8.61	8.5
Tb	0.03	1.04	0.7	0.51	0.66	0.6	0.61	0.06	0.78	0.7	0.07	0.35	0.56
Tm	0.2	0.2	1.3	1.54	0.65	0.59	1.5	0.55	1.4	1.4	1.37	1.46	1.36
Yb	0.2	0.2	1.45	1.06	0.74	0.64	1.7	0.61	1.69	1.27	1.2	0.93	1.88
Lu	0.01	0.01	0.2	0.14	0.03	0.32	0.34	0.02	0.25	0.2	0.2	0.21	0.23
Σ REE	154.72	58.62	79.08	105.55	106.15	131.53	98.83	112.74	86.59	85.10	118.01	42.85	72.42
Σ LREE	119.46	51.41	67.75	94.81	91.64	119.40	67.90	96.09	56.00	68.30	97.03	27.50	53.90
Σ MREE	34.85	6.80	8.38	8.00	13.09	10.58	27.39	15.47	27.25	13.93	18.21	12.75	15.05
Σ HREE	0.41	0.41	2.95	2.74	1.42	1.55	3.54	1.18	3.34	2.87	2.77	2.60	3.47
Eu/Eu*	0.04	1.62	1.16	0.84	1.00	0.93	0.43	0.64	0.42	0.71	0.75	0.71	0.58
Sr/Sr*	0.17	0.36	0.22	0.13	0.25	0.12	0.21	0.15	0.41	0.21	0.15	0.73	0.25
Zr/Zr*	0.04	0.09	0.13	0.08	0.05	0.06	0.10	0.06	0.29	0.07	0.03	0.06	0.13
(La/Lu)n	351.54	133.22	10.17	19.36	71.43	8.16	5.73	101.79	12.36	8.40	10.46	4.66	8.02
(La/Yb)n	113.73	43.10	9.08	16.55	18.74	26.39	7.41	21.60	11.83	8.56	11.28	6.81	6.35
(La/Sm)n	0.63	2.33	3.13	3.94	2.28	3.15	2.63	2.18	7.56	2.88	1.63	2.18	2.30
(Gd/Yb)n	4.94	4.98	1.43	1.88	5.47	4.66	9.85	10.99	10.85	5.33	5.65	7.38	3.60
(Tb/Yb)n	0.70	24.34	2.26	2.25	4.17	4.39	1.68	0.46	2.16	2.58	0.27	1.76	1.39

(Ce/Yb)n	80.62	37.82	5.44	11.13	15.77	23.29	4.94	18.03	3.01	5.21	10.03	2.46	2.84
"r"	291.37	125.39	22.97	34.60	64.54	77.03	19.18	81.43	16.77	23.80	35.03	10.58	15.53
Ti	2840.24	4970.41	5680.47	6035.50	5502.96	6094.67	6035.50	5147.93	4319.53	5857.99	11124.26	6804.73	5088.76
Ti/Cr	71.01	124.26	49.40	90.08	98.27	41.46	163.12	20.51	65.45	40.96	505.65	158.25	42.41
Mg# (mole %)	0.68	0.60	0.67	0.62	0.67	0.67	0.65	0.72	0.73	0.71	0.54	0.65	0.75
CIPW norm (wt %)													
Quartz	17.95	19.16	16.82	12.26	8.28	12.06	9.84	7.78	6.42	5.66	2.93	2.29	0.00
Orthoclase	20.03	7.17	10.22	15.25	8.91	9.26	10.01	15.41	4.78	4.56	9.42	5.80	19.83
Albite	39.16	44.24	33.20	36.71	39.72	29.84	32.37	27.82	35.18	33.09	37.59	35.46	34.39
Anorthite	12.68	16.75	20.88	19.19	24.05	26.22	26.67	24.44	27.23	28.08	25.39	32.26	17.78
Plagioclase	51.84	60.99	54.08	55.91	63.77	56.07	59.04	52.26	62.41	61.17	62.98	67.72	52.17
Nephline	0.00	0.00	0.00	0.00	0.00	0.00	0.00	0.00	0.00	0.00	0.00	0.00	3.45
Corundum	0.92	0.00	0.00	0.00	0.00	0.00	0.00	0.00	0.00	0.00	0.00	0.00	0.00
Diopside	0.00	4.09	2.99	0.53	4.25	4.11	3.12	0.74	12.58	6.83	3.28	3.15	4.02
Hypersthene	5.12	2.79	9.81	9.50	8.69	12.05	11.67	18.04	9.02	15.70	11.86	14.31	0.00
Pyroxene	5.12	6.87	12.80	10.03	12.94	16.16	14.79	18.78	21.60	22.52	15.15	17.45	4.02
Olivine	0.00	0.00	0.00	0.00	0.00	0.00	0.00	0.00	0.00	0.00	0.00	0.00	14.88
Magnetite	2.91	3.46	3.61	3.76	3.56	3.71	3.71	3.49	3.31	3.67	4.91	3.89	3.52
Ilmenite	0.93	1.63	1.84	1.99	1.79	1.98	1.97	1.68	1.42	1.91	3.58	2.21	1.68
Apatite	0.31	0.73	0.63	0.81	0.75	0.77	0.66	0.61	0.07	0.52	1.05	0.63	0.45

"r" = $\sum$ LREE / $\sum$ HREE

Geochemical classification using SiO_2 versus alkalies diagram (Irvine and Baragar, 1971) shows that the studied metagabbros and doirite plot mostly in the subalkaline field except two samples of metagabbro and one sample of diorite in alkaline field as a result of enrichment of alkalies (Fig. 4c). The sample data plot in both the calc-alkaline and tholeiitic fields of Irvine and Baragar (1971) and Miyashiro (1974) (Figs. 4d & 4e) for the studied diorite and metagabbro respectively. Most major and trace elements of these rock suites exhibit more or less smooth variation trends with increasing SiO_2 (Fig. 5a & 5b), as a result of simple fractional crystallization. Al_2O_3, FeO^t, MgO, CaO, Sr and V all show strong negative correlation with SiO_2, whereas Na_2O, K_2O, Ba, Rb and Zr show strong positive correlations. Selected Harker diagrams show clear trends for some major and trace elements (e.g. TiO_2, Cr and Ni).

The El-Fringa metagabbros-diorite complex exhibits enrichment in light REE depletion in the middle and heavy REE based on the chondrite- and N-type MORB-normalized REE patterns (Figs. 6a & 6b), this suggests either the presence of residual garnet in the source or a light REE enriched source. Some samples of the studied metagabbros and diorites exhibit positive Eu-anomalies due to plagioclase accumulations which led to the abundance of Eu and light REE, and helped in diluting the middle and heavy REE (Hassanipak et al, 1996), while one sample of diorite rocks shows negative Eu-anomaly due to the dominance of the incompatible element-rich melt. These figures also show that these rocks have higher REE enrichment compared to the primitive compositions, indicating that the range in REE enrichment is probably the result of a fractionating basaltic magma within each group of samples rather than variable degrees of partial melting in the mantle source region.

The metagabbro-diorites show pronounced enrichment in large-ion lithophile elements (LILEs) (such as Rb, Ba, and Th), and depletion in high-field strength elements (HFSEs) (such as, Zr and Ti).

The primitive mantle-normalized multi-elemental patterns (Fig. 6c) of the studied metagabbro-diorite complex show positive Sr-anomalies and no Zr-anomalies. Generally, this feature may suggest contamination of the gabbroic magma by components added to the mantle source by subduction zone fluids or retention of these elements in the source during partial melting (Wilson, 1989). Also, the more incompatible elements Y, Tb & Yb are depleted and have flat patterns.

a

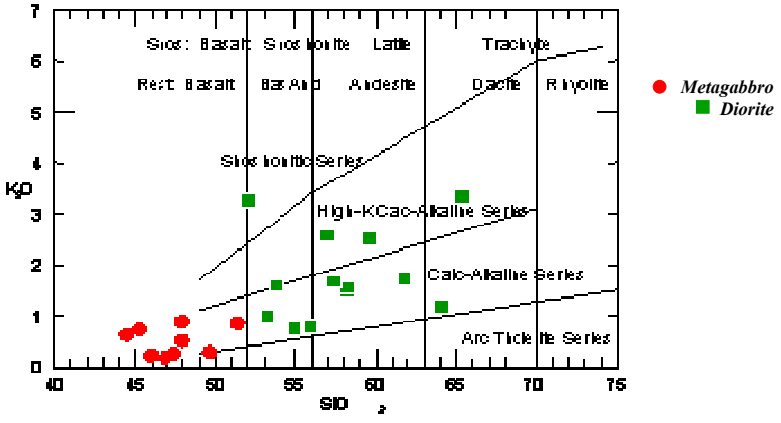

b

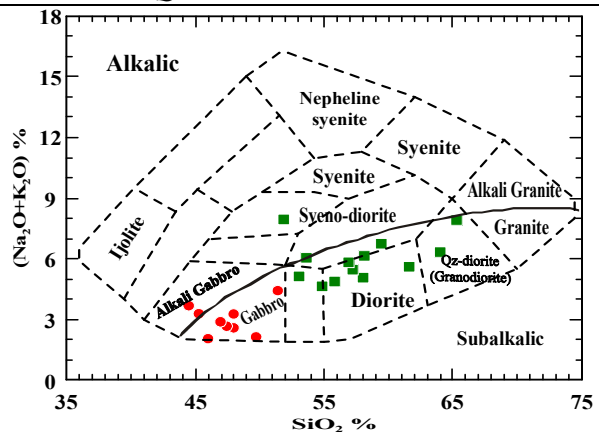
Alkalic
Nepheline syenite
Syenite
Syenite
Alkali Granite
Syeno-diorite
Granite
Ijolite
Qz-diorite (Granodiorite)
Alkali Gabbro
Gabbro
Diorite
Subalkalic
(Na2O+K2O) %
SiO2 %
18
15
12
9
6
3
0
35
45
55
65
75

c

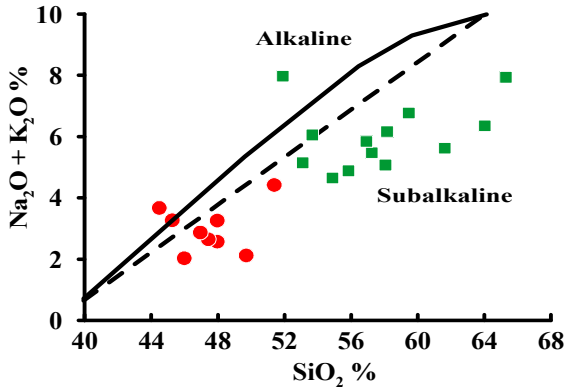
Alkaline
Subalkaline
Na2O + K2O %
SiO2 %
10
8
6
4
2
0
40
44
48
52
56
60
64
68

d

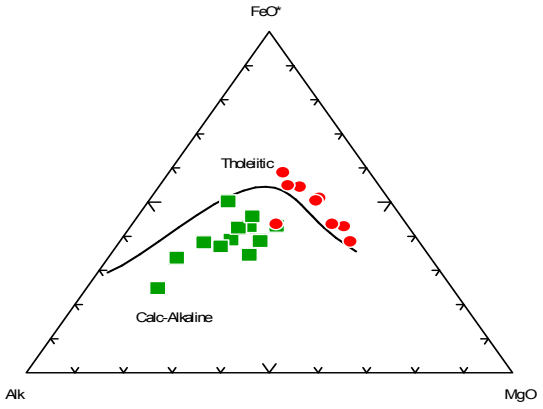
FeO*
Tholeiitic
Calc-Alkaline
Alk
MgO

e

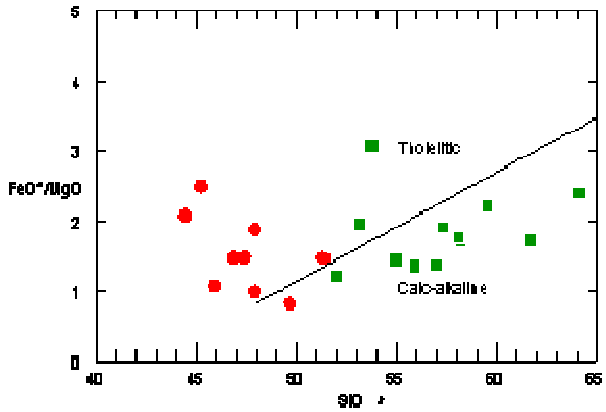

Fig. (4): a) SiO_2-K_2O discrimination diagram of Peccerillo and Taylor (1976), b) TAS diagram after Cox et al. (1979). The dividing line between alkalic and subalkalic after Miyashiro (1978), c) Total alkalies versus silica diagram. Alkaline/subalkaline dividing curved line after Irvine and Baragar (1971), dashed line after Mac Donald (1968), d) Plot of alkalis-FeO^t (total iron as ferrous iron)-MgO for the studied rocks with line separating calc-alkaline and tholeiitic rocks after Irvine and Baragar (1971), e) Tholeiitic- calc alkaline discrimination diagram of Miyashiro (1974).

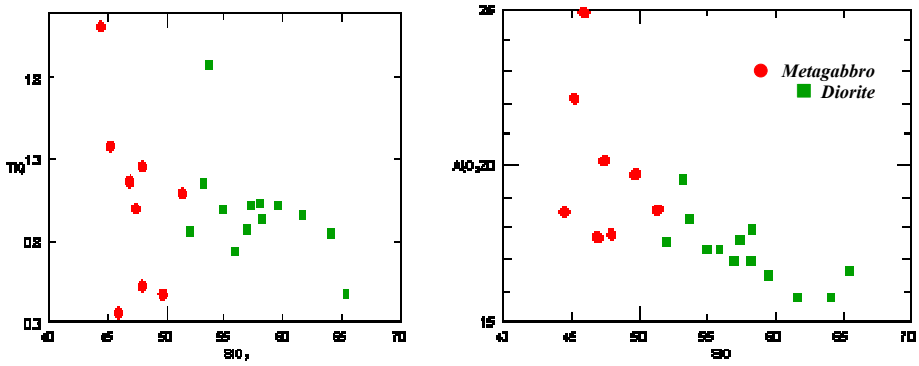

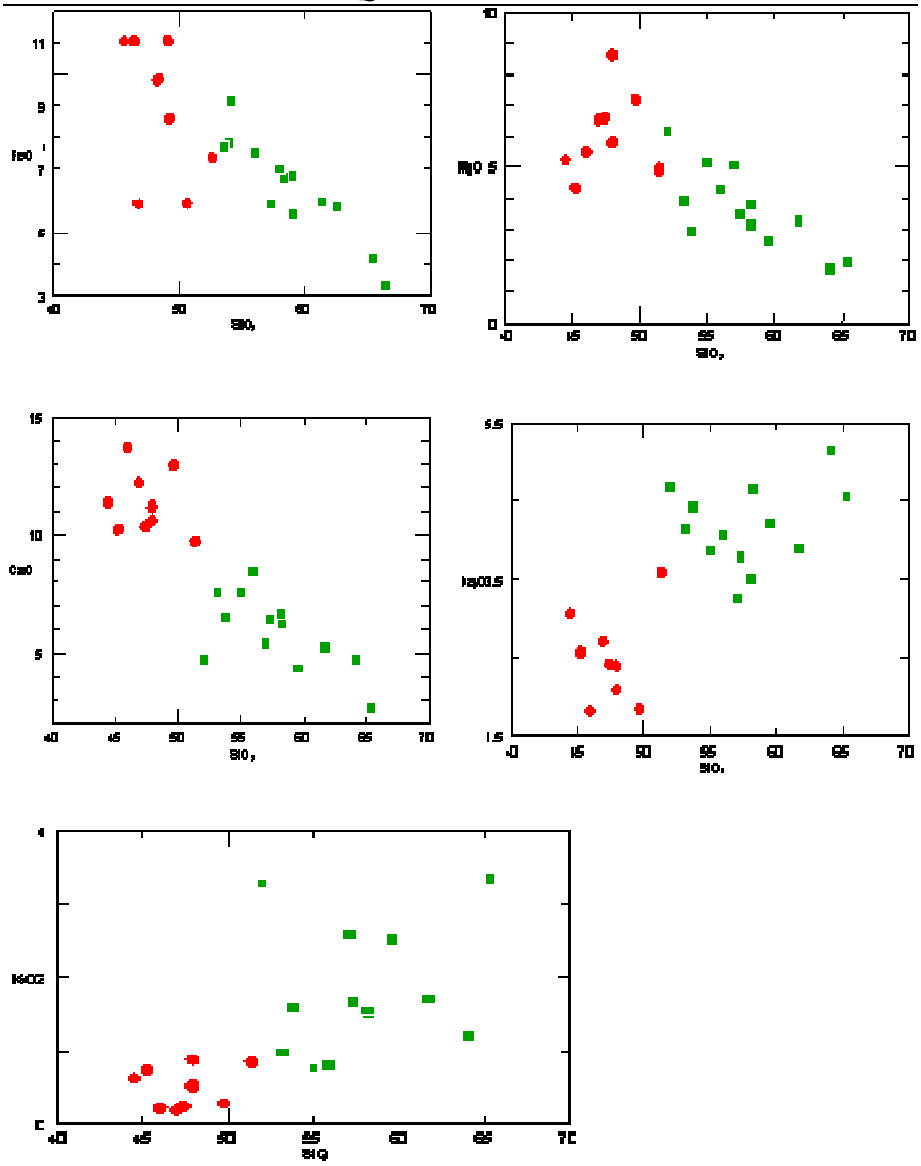

Fig. (5a) Harker variation diagrams for major elements (wt %) of the samples from El-Fringa metagabbro-diorite complex.

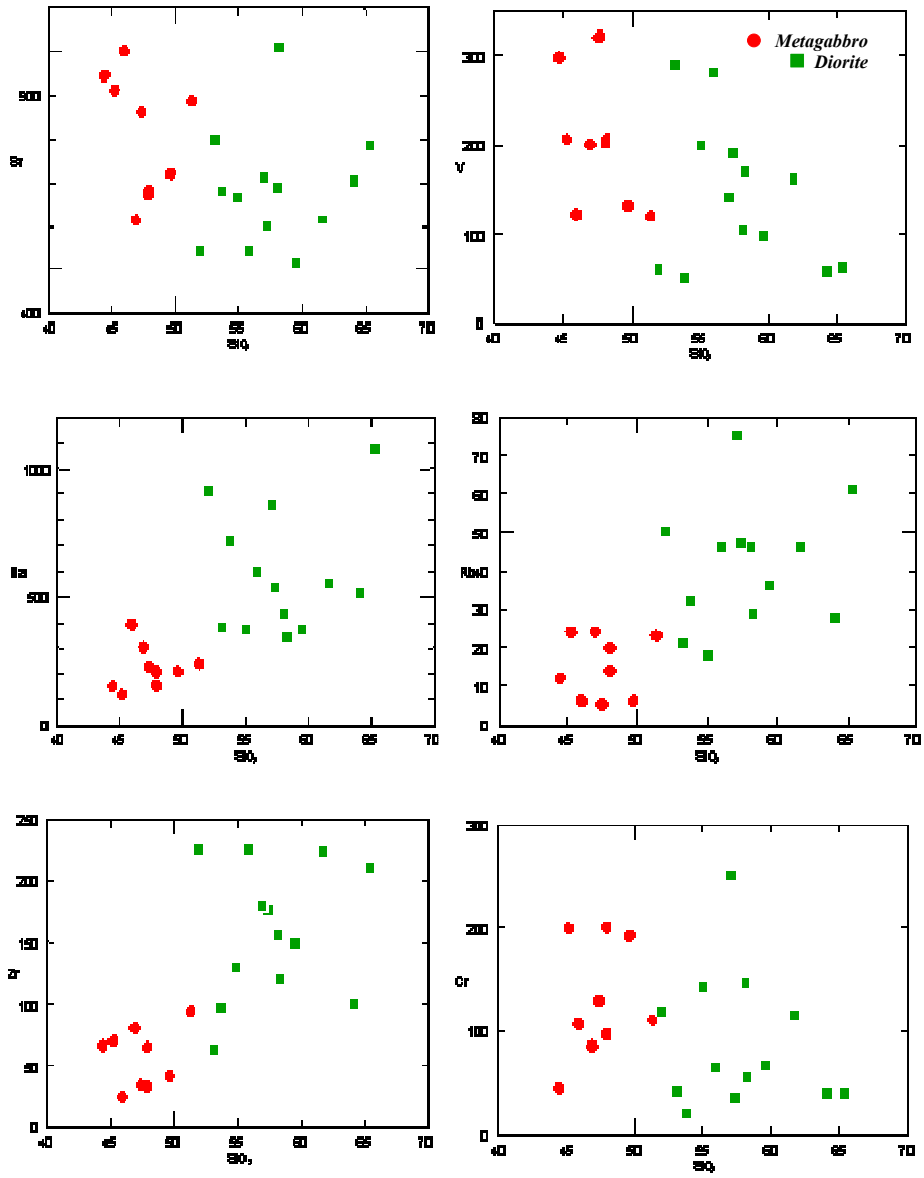
Metagabbro
Diorite
Sr
V
Ba
Rb
Zr
Cr
SiO2

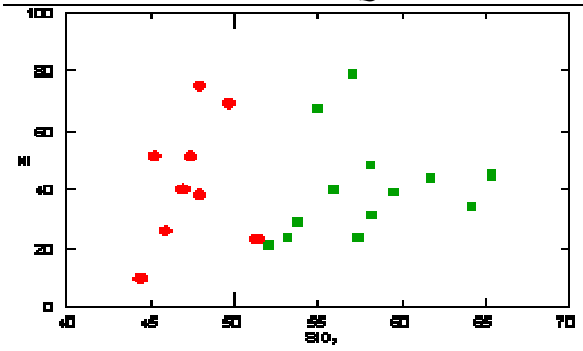

Fig. (5b) Harker variation diagrams for same trace elements (ppm) of the samples from El-Fringa metagabbro-diorite complex

Tectonic setting and petrogenesis

The investigated metagabbro-diorite complex displays island-arc characteristics (TH and CA) based on Miyashiro and Shido (1975) who suggested the relation between Ni and FeO^t/MgO (Fig. 6d) to investigate the MORB and island-arc nature. The majority of the studied rocks has more affinity with island-arc series than modern ocean-floor or marginal basin basalts, although it is well being noticed that the distribution of the data points in this diagram (suggested by Pearce, 1975), is strongly influenced by the geometry of the Ti-depletion and Cr-enrichment fractionation. The present rock samples compare more favorably with the island-arc chemistry. This point is illustrated by Ti-Cr and Ni-Ti/Cr discrimination plots (suggested by Beccaluva et al., 1975) of Fig. (7a & 7b), which demonstrate their island-arc affinity.

The Cr-Y plot devised by Pearce (1980) is one of the classic discrimination diagrams that had long been used to characterize mafic suits of ambiguous origin, in which the investigated rock samples fall mostly with VAB (volcanic-arc basalt) with only one sample falling in MORB (mid-ocean ridge basalt) field (Fig. 7c).

Pearce and Cann (1973) used Ti-Zr-Sr diagram to distinguish between oceanic floor, island-arc and calc-alkaline basaltic suites, the examined metagabbro and diorite are located within the fields of island-arc basalts and calc-alkaline basalt (Fig. 7d), therefore the rocks

of metagabbro prove to have island-arc affinity while the diorite rocks to have calc-alkaline affinity.

The geochemical features presented can help to resolve the controversy regarding the tectonic setting of the present mafic intrusion; it represents a product of arc magmatism in a subduction zone environment. These rocks show pronounced enrichment in large-ion lithophile elements (LILEs) (such as Rb, Ba, and Th), and depletion in high-field strength elements (HFSEs) (such as, Zr and Ti) with increasing SiO_2. Such features are consistent with modern calc-alkaline island-arc suites. The parental magma of the metagabbro-diorite complex is, thus, believed to be generated by partial melting of mantle wedge above subduction zones that have been previously metasomatised by slab-derived fluids (Saunders et al., 1980). The presence of cumulate features and the decreasing in Ni, Cr and MgO abundances are consistent with significant clinopyroxene (and/or olivine) and plagioclase fractionation, so crystal/melt fractional crystallization may explain the geochemical variations of the present metagabbro-diorite pluton.

a

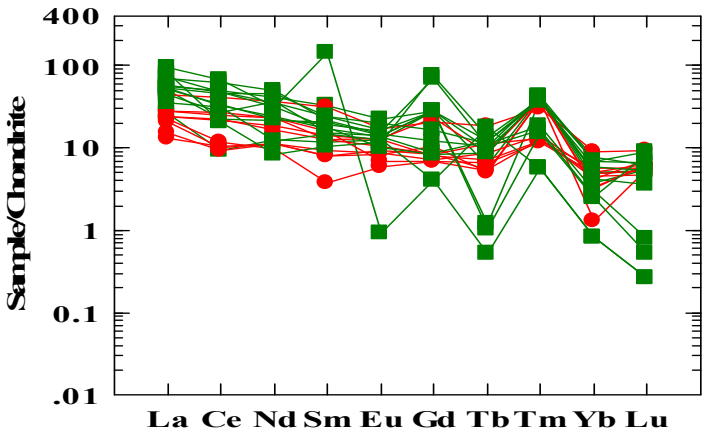

b

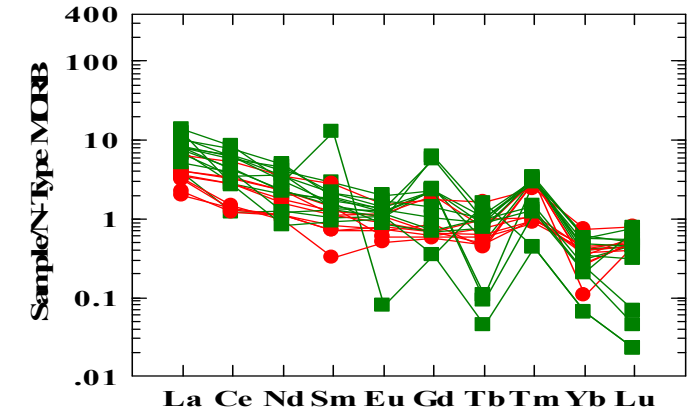

c

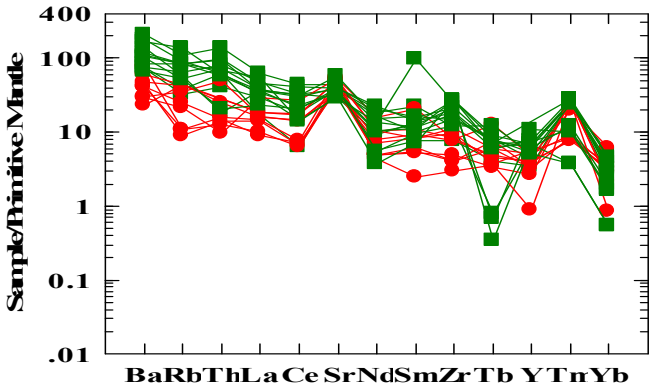

d

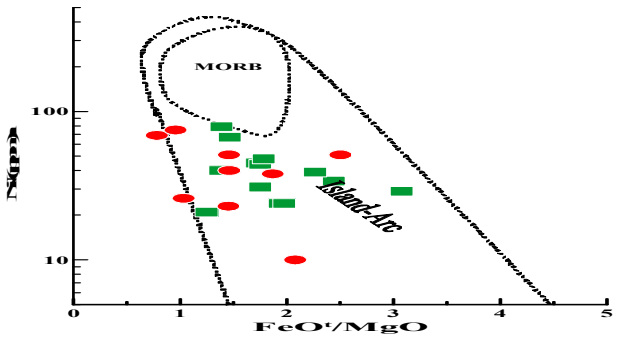

Fig. (6): a) Chondrite-normalized REE patterns for the studied rocks (Nakamura, 1974), b) N-type MORB-normalized patterns (Sun and McDonough, 1989), c)

Primitive mantle-normalized trace element patterns (Wood et. al., 1979), d) Ni-FeOt/MgO diagram for the studied rock types, after Miyashiro and Shido (1975).

Discussion and conclusions

The present study deals with the petrology and geochemistry of El-Fringa metagabbro-diorite complex at South Sinai of Egypt to an attempt to clarify their petrogenesis and tectonic setting. This metagabbro-diorite complex crops out at the northwest district of Wadi El-Raiyan (a tributary from Wadi Sa'al) and forms moderately and rugged outcrops of Newproterozoic igneous and metamorphic rocks. The studied area is underlain mainly by metagabbro-diorite intrusive complex intruded in Sa'al metavolcanics and latter intruded by late- to post-tectonic granitoid rocks. These metavolcanics characterized by at Wadi El-Raiyan; acidic in composition; calc-alkaline to sub-alkaline; regionally metamorphosed up to the greenschist facies and are related to the calc-alkaline island arc metavolcanics of the central Eastern Desert of Egypt (Bentor, 1985).

The investigated metagabbro-diorite complex occurs as a small stock, intrudes Sa'al metavolcanics at the start and north of Wadi El-Raiyan and also a nearly circular stock-like intrusion surrounding the voluminous granite of Wadi Saal. It is represented by heterogeneous mafic and intermediate rock varieties comprising hornblende metagabbro and diorite to quartz-diorite based on the color index, textures and mineral proportions. The pyroxenehornblende metagabbros consist mainly of calcic plagioclase, hornblende and pyroxene with subordinate amount of biotite and quartz with some accessory ilmenite, magnetite, apatite and pyrite. On the other hand, the diorite is composed essentially of plagioclase (andesine to oligoclase) and green hornblende with subordinate amount of actinolite, quartz and minor biotite, iron-titanium oxides, titanite and epidote.

Geochemically, the studied metagabbro have markedly enrichment in TiO_2, Fe_2O_3, MgO and CaO contents relative to those of diorite, whereas it has low contents of Al_2O_3, SiO_2 and K_2O than diorite. El-Fringa metagabbro-diorite complex is medium-to high-K calc-alkaline and meta- to mildly peralurninous. The studied metagabbro is tholeiitic with subordinate alkalic varieties, while the diorite is calc-alkaline affinity, major and trace element chemistry indicates that they

are genetically unrelated. It is suggested that the metagabbro-diorite complex was probably formed by fractional crystallization of a basaltic magma derived by partial melting of a metasomatised upper mantle in an island-arc setting.

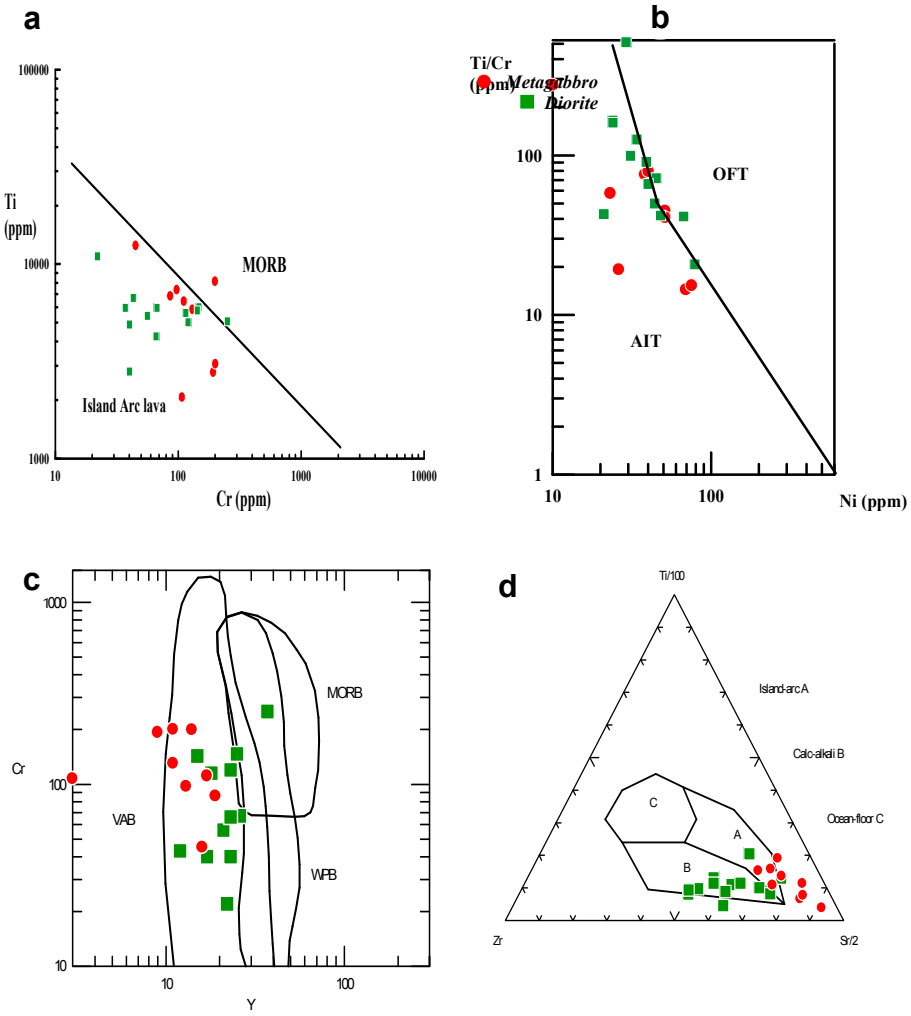

Fig. (7): a) Ti versus Cr diagram for the studied rock types. Fields after Pearce (1975), b) Ti/Cr-Ni diagram after Beccaluva et al. (1975), c) Cr-Y diagram after Pearce (1980), d) Ti/100-Zr-Sr/2 ternary diagram after Pearce and Cann (1973).

This complex is generally enriched in light REE with distinctly positive Eu anomalies for all samples of metagabbro and some samples of diorite and slight negative Eu anomalies for other samples of diorite. The rocks are generally depleted in HREE indicates the presence of garnet in the source (Weaver and Tarney, 1981). Systematic increase in total REE abundances from the least evolved gabbro to the most evolved gabbro and diorite can be explained in terms of fractional crystallization.

Finally, the geochemical characteristic features presented proved that, the mafic intrusion of El-Fringa area at Wadi Sa'al, southern Sinai may represent a product of island arc magmatism in a subduction zone environment.

Acknowledgements

We are grateful to Associate Prof. B. Zoheir (Benha University) for his suggestions that greatly improved the initial version of this manuscript.

References

Abdel-Karim, A.M., El-Awady, A. A., Helmy, H., Al-Afandy, A.H. and Abdalla, Sh. 2011: Younger Gabbros from Egypt: a transition from tholeiitic to alkaline basaltic magma and from arc to within plate rifting regime. The 6th Environmental Conference, Faculty of Science, Zagazig University, Zagazig, P. 194-220.

Abdel Rahman, A.M., 1990: Petrogenesis of early-orogenic diorites, tonalites and post-orogenic trondhjemites in the Nubian shield. Journal of Petrology, v. 31, pp. 1285–1312.

Abdel Rahman, A. M. and Doig, R. 1987: The Rb-Sr geochronological evolution of the Ras Gharib segment of the northern Nubian shield. Journal of Geological Society, London, v. 144, pp. 577–586.

Akkad, M. K. and El Ramly, M. F., 1960: Geological history and classification of the basement rocks of central Eastern Desert of Egypt. Annals of Geological Survey, Egypt, v. 9, pp. 24.

Basta, F. F. (1998): Mineralogy and petrology of some gabbroic intrusions in Sinai and the Eastern Desert, Egypt. Annals Geological Survey, Egypt, v. 21, pp. 239–271.

Beccaluva, L., Ohnenstetter, D., and Ohnenstetter, M., 1975: Geochemical discrimination between ocean-floor and island-arc tholeiites - application

to some ophiolites. Canadian Journal of Earth Science., v. 16(9), p., 1874-1882.

Bentor, Y. K., 1985: The crustal evolution of the Arabo-Nubian Massive with special reference to the Sinai Peninsula. Precambrian Research, v. 28, pp. 1–74.

Cox, K. G., Bell J. D. and Pankhurst, R. J., 1979: The interpretation of igneous rocks. London Allen and Unwin., 450 p.

De la Roche, H., Leterrier, J., Grandcìaude, P. and Marchal, M., 1980: A classification of volcanic and plutonic rocks using R1–R2 diagram and major element analyses – its relationships with current nomenclature. Chemical Geology, v. 29, pp. 183–210.

El Gaby, S., List, F. K and Tahrani, R., 1988: Geology, evolution and metallogenesis of the Pan-African belt in Egypt. In El-Gaby, S. and Greilling, R. O. (eds.), The Pan- African belt of Northeast Africa and Adjacent Areas. Fredr, vieweg & Sohn, Braunschweig/ Wiesbaden.

El Metwally, A.A. (1993): Microgranular enclaves in the Pan African I-type granites from the Sinai Massif: Petrology, Mineralogy and geochemistry. Journal of African Earth Science, v. 17(1), pp. 95-110.

El Metwally, A.A., 1997: Petrogenesis of metagabbro-diorite complex from SW Sinai massif: Implications for subduction at Neoproterozoic continental margin. Proceedings of Egyptian Academic Sciences, v. 47, pp. 273-295.

El Ramly, M. F., 1972: A new geological map for the basement rocks in the Eastern and Southwestern Desert of Egypt, Scale 1: 1000000. Annals of Geological Survey, Egypt, v. 11, pp. 1-18.

Essawy, M.A., El-Metwally, A.A., Katta, L.A. and Darwish, N.K., 1997: Younger granites and pegmatites from Taba area, southeastern Sinai, Egypt. Egypt. Journal of Geology, v. 41 (1), pp. 495-518.

Ghoneim, M.F., Lebda, E.M., Abdel-Karim, A.M. and N. Nasralla (2008): On the Plutonities of the Subduction Regime south Sinai: Discrimination and Modeling. The 8th Inter. Conf. on Geochemistry, Alex. Univ., Abst., 23-24.

Gill, J. B., 1981: Orogenic andesites and plate tectonics. Springer, Berlin Heidelberg, New York, 390 p.

Hassanipak, A. A., Ghazi, A. M., and Wampler, J. M., 1996: REE characteristics and K/Ar ages of the Band-Ziarat ophiolite complex, southeastern Iran. Canadian Journal of Earth Science, v. 33, pp. 1534-1542.

Hashad, A. H., 1980: Present status of geochronological data on the Egyptian basement complex. Bulletin of Applied Geology, King Abdul Aziz University, Jeddah, v. 3, pp. 31-46.

Hassan, M. A. and Hashad, A. M., 1990: Precambrian of Egypt. In: Said R. (ed) The geology of Egypt. Balkema, Rotterdam.

Hassen, I. S., Ibrahim, S. K. and Elemer, P. M., 2004: Evolution and origin of the metavolcanics at Wadi Saâl area, south Sinai, Egypt. Annals of Geological Survey, Egypt, v. 27, pp. 61–78.

Hassanen, H. A., 1989: Geochemistry and petrogenetic evolution of a Late Precambrian metagabbro-diorite complex, South-Eastern Sinai. 1st Conference on Geochemistry, Alex University, Egypt, pp. 118–139.

Irvine, T. N., and Baragar, W. R. A., 1971: A guide to chemical classification of the common volcanic rocks. Canadian Journal of Earth Science, v. 8, p. 523-548.

Madbouli, M. E., 1991: Petrology and geochemistry of some mafic and ultramafic rocks of Sinai, Egypt. M. Sc. thesis, Cairo University, Egypt.

Mac Donald, G. A., 1968: Composition and origin of Hawaiian lavas: Memorial of Geological Society of American, v. 116, pp. 477-522.

Miyashiro, A., 1974: Volcanic rock series in island arcs and active continental margins. American Science, v. 274, pp. 321-355.

Miyashiro, A., 1978: Nature of alkalic volcanic rocks series. Contribution to Mineralogy and Petrology, v. 66, pp. 91-104.

Miyashiro, A., and Shido, F., 1975: Tholeiitic and calc-alkalic series in relation to the behaviors of titanium, vanadium, chromium and nickel: American Science, v. 275, p. 265-277.

Nakamura, M., 1974: Determination of REE, Ba, Fe, Mg, Na and K in carbonaceous and ordinary chondrites. Geochimica et Cosmochimica Acta, v. 38, pp. 757-773.

Pearce, J. A., 1975: Basalt geochemistry used to investigate post-tectonic environments in Cyprus: Tectonophysics, v. 25, p. 41-67.

Pearce, J. A., 1980: Geochemical evidence for the genesis and eruptive setting of lavas from Tethyan ophiolites. In: A. Panayiotou (ed.); Ophiolites: Proceedings International Ophiolite Symposium Cyprus, 1979, pp. 261-272.

Pearce, J. A., and Cann, J. R., 1973: Tectonic setting of basic volcanic rocks determined using trace element analyses. : Earth and Planetary Science Letters, v. 19, pp. 290-300.

Peccerillo, A. and Taylor, S.R. (1976): Geochemistry of Eocene calc-alkaline volcanic rocks from the Kastamonu area, north Turkey. Contributions to Mineralogy and Petrology 58, 63–81.

Pindell, J. and Kennan, L. (2001): Kinematic evolution of the Gulf of Mexico and Caribbean. In: Fillon, R.H., Weimer, P., Lowrie, A., Pettingill, H., Phair, R. L., Roberts, H.H., van Hoorn, B. (eds.). Petroleum Systems of Deep-Water Basins: Global and Gulf of Mexico Experience. Gulf Coast Section Society of Economic Palaeontologists and Mineralogists. 21st Annual Bob Perkins Research Conference, Petroleum Systems of Deep-Water Basins, pp. 193-220.

Saunders, A. D., Tarney, J. and Weaver, S. D., 1980: Transverse geochemical variations across the Antarctic Peninsula: implications for the genesis of calc alkaline magmas. Earth Planetary Science Letters, v. 46, pp. 344-360.

Sun, S. S., and MC Donough, W. F. (1989): Chemical and isotopic systematics of oceanic basalts: implications for mantle composition and processes. In Saunders, A.D., and Norry, M.J. (eds). Magmatism in the oce an basins. Special Publication of Geological Society of London, v. 42, pp. 313-345.

Takla, M. A., Basta, F. F., Madbouly, M. I. and Hussein, A. A. (2001): The mafic-ultramafic intrusions of Sinai, Egypt. Annals of Geological Survey, Egypt, v. 24, pp. 1–40.

Vail, J. R. (1985): Pan-African (Late Precambrian) tectonic terrains and the reconstruction of the Arabian-Nubian Shield. Geology 13, 839-842.

Weaver, B.L. and Tarney, J., 1981: The Scourie dyke suite: Petrogenesis and geochemical nature of the Proterozoic sub-continental mantle. Contributions to Mineralogy and Petrology 78, 175-188.

Wilson, M. (1989): Igneous Petrogenesis. Unwin Hyman, London, 466.

Wood, D. A., Tarney, J., Saunders, A. D., Bougault, H., Joron, J. L., Treuil, M., and Cann, J. R., 1979: Geochemistry of basalts drilled in the north Atlantic by IPODL eg 49: implications for mantle heterogeneity. Earth Planetary Science Letters, v. 42, pp. 77-97.